THE JOURNAL OF PHYSICAL CHEMISTRY A

pubs.acs.org/JPCA Article

The Loss of Size Sensitivity in *para*-Hydrogen Clusters Due to the Strong Quantum Delocalization

Bridgett H. Kohno and Vladimir A. Mandelshtam*

Cite This: *J. Phys. Chem. A* 2020, 124, 8766–8777 Read Online

ACCESS | Metrics & More | Article Recommendations

ABSTRACT: *para*-Hydrogen $(pH_2)_N$ clusters have been the focus of numerous computational studies. Originally motivated by the possibility of observing superfluidity, these studies also revealed rich and complex structural properties of $(pH_2)_N$. However, their structural analysis was typically limited to attempts to identify "magic number clusters" by computing their ground state energies E_N and the chemical potential $\mu_N = E_N - E_{N-1}$ as a function of N. This was followed by structural analysis based on an ill-defined radial density profile. Surprisingly, however, there were remarkable discrepancies between the results reported in the literature for cluster sizes beyond approximately $N = 25$, and this ambiguity remained unsettled until now. In the present paper, we apply the diffusion Monte Carlo method to resolve inconsistencies in cluster sizes within the range ($N = 24–28$). Here, we try to avoid speculations based on the highly demanding energy calculations whose numerical accuracy harbors ambiguity. Instead, we focus on the direct and unambiguous structural analysis of the ground state wavefunctions, which supports the conclusion that the clusters are structurally the same in the size range considered. That is, there are no magic number clusters at least in the range $N = 24–28$, contrary to what some of the previous publications have suggested. This lack of size sensitivity of *para*-hydrogen clusters is a direct consequence of the strong quantum delocalization in these systems.

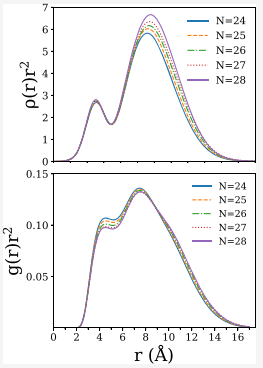

INTRODUCTION

Studies of *para*-hydrogen clusters $(pH_2)_N$ over the past several decades were mainly motivated by the speculation that the cluster form of hydrogen could display superfluidity, unlike bulk hydrogen.[1,2] However, hydrogen clusters possess very strong nuclear quantum effects (NQEs) that make them interesting to study beyond whether or not superfluidity could be observed. In fact, the strength of the NQEs in this system is second only to helium out of all molecular and atomic systems.

A truly accurate description of molecular hydrogen requires a many-body potential, which should, in particular, include the stiff H–H degrees of freedom. However, it was argued that a central two-body potential where the H_2 molecules are treated as point particles is sufficient unless the intramolecular dynamics are important.[3,4] This "united-atom" model is believed to provide a qualitatively correct description of this challenging system, while also reducing the computational cost by at least an order of magnitude compared to the "all-atom" model. This makes it possible to study clusters of relatively large sizes.

There are two pair potentials to describe hydrogen clusters: the Silvera–Goldman (SG)[3] and the Buck[4] pair potentials, with the SG potential being somewhat more popular. These two potentials are similar to one another, as well as to the more simple Lennard–Jones (LJ) potential with an appropriate choice of the LJ parameters. In this paper, we choose to use the SG potential and compare our results to those reported in the literature. We also reference the facts established from the heavily studied LJ clusters, specifically quantum LJ clusters.[5–10]

Given the potential energy surface (PES), the main approaches to study *para*-hydrogen clusters have been the diffusion Monte Carlo (DMC),[11–14] the path integral Monte Carlo (PIMC),[8,15] and the path integral ground state (PIGS)[16–23] methods.

A major theme in many publications on *para*-hydrogen clusters beyond the topic of superfluidity has been the identification of "magic number clusters," i.e., the clusters $(pH_2)_N$ that would be "especially stable" relative to those with similar sizes N. Although a correct assessment of a cluster's stability must rely on its free energy, at sufficiently low temperatures, this can be reduced to an analysis of the size dependence of the ground state energy E_N. In the classical limit ($\hbar^2/m \to 0$), this comes down to an analysis of the global energy minima. It is therefore appropriate to draw insight from studies of LJ_N clusters in this limit, which have been studied extensively and are well understood. For example, the equilibrium structures of classical LJ clusters have a well-

Received: August 3, 2020
Revised: September 16, 2020
Published: September 22, 2020

https://dx.doi.org/10.1021/acs.jpca.0c07107
J. Phys. Chem. A 2020, 124, 8766–8777

understood size dependence, which is manifested as numerous spikes in the chemical potential $\mu_N = E_N - E_{N-1}$ (see refs 24−26). Note that the icosahedral symmetry is the dominating motif in global minima structures of small LJ clusters with several exceptions. Complete icosahedral structures belong to LJ_{13}, LJ_{55}, and LJ_{147} clusters, which correspond to the most pronounced minima of the chemical potential μ_N. Meanwhile, the clusters of intermediate sizes, i.e., those with an incomplete icosahedral outer shell, also show strong size sensitivity, albeit with smaller fluctuations of the μ_N dependence. Furthermore, there are a few other magic number clusters (e.g., LJ_{38}, LJ_{75}, LJ_{98}, etc.) that have highly symmetric but non-icosahedral global minima.

It seems natural to assume that the SG_N and LJ_N clusters display similar magic number patterns due to the similarity between SG and LJ potentials. However, to the best of our knowledge, there has not been a both systematic and quantitatively reliable study of magic number patterns for quantum LJ_N clusters. Instead, we find references in the literature to the NQEs washing out the size sensitivity, specifically in the LJ clusters, due to the strong quantum delocalization.[5−7,10]

In LJ systems, NQEs are conveniently quantified by the de Boer quantum delocalization length $\Lambda := \hbar/(\sigma\sqrt{m\varepsilon})$, where m is the particle mass and ε and σ are the parameters of the LJ pair potential. For example, the following systems, Xe_N, Ar_N, Ne_N, $(D_2)_N$, and $(H_2)_N$, respectively correspond to the following approximate values of Λ: 0.01, 0.03, 0.095, 0.19, and 0.28. It has been shown that an increase in Λ results in structural changes in LJ_N clusters, which are generally accompanied by an increase in disorder due to quantum fluctuations. Moreover, quantum-induced transitions from changing Λ have the same origin as the thermally-induced transition in the classical systems, where both transitions result from the competition between energetic and entropic effects.[5,7,10] For example, none of the highly symmetric non-icosahedral structures survive in the quantum Ne_N clusters, (i.e., for systems that are much less quantum than the $(pH_2)_N$ clusters). References 7, 10, 14 further demonstrate that even the Mackay icosahedral symmetry does not survive in small $(H_2)_N$ and even $(D_2)_N$ clusters. In particular, the structural analysis of the ground state of LJ_{38} upon continuously changing Λ demonstrates that the ground state of $(H_2)_{38}$ is completely delocalized over all symmetry motifs; i.e., it is liquid-like. Meanwhile, the less quantum $(D_2)_{38}$ is localized in a single local energy minimum (or possibly in a few minima separated by low energy barriers). Notably, this local minimum is one of the many highly disordered but otherwise structurally indistinguishable minima that all compete for the ground state. This situation is unique to $(D_2)_N$ clusters and is particularly intriguing. However, it is also extremely difficult to investigate numerically and, as such, deserves special attention.

We now turn to reviewing some results and conclusions specifically on pH_2 clusters reported in the literature by other groups over the past decades. We will highlight studies whose motivations coincide with searching for magic number clusters and are directly related to the present work. However, by no means should this be regarded as a comprehensive literature review since that is beyond the scope of the present paper.

In Figure 1 we show selected results from chemical potential computations on $(pH_2)_N$ clusters obtained from different groups and their respective methods.[12,13,17,23] This figure demonstrates that there is a disagreement between different

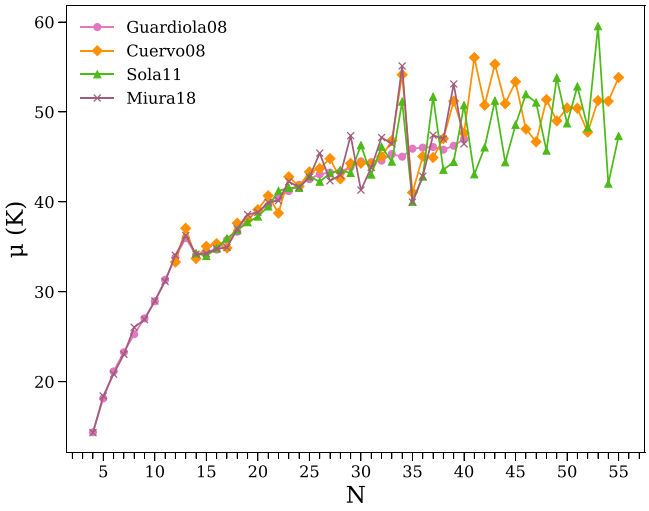

Figure 1. Chemical potential μ_N as a function of cluster size reported in various publications: Guardiola08 (ref 12, using DMC-IS), Cuervo08 (ref 12, using PIGS), Sola11 (ref 13, using DMC-IS), and Miura18 (ref 23, using VPI, a variant of PIGS).

calculations, particularly from around cluster size $N \approx 25$, which increases with N. We find this disagreement unsurprising. Although in-principle-exact, each of the methods is plagued with numerical convergence problems associated with both the systematic and statistical errors that are very difficult to assess. For example, the main source of systematic errors in the PIMC method is the use of a finite number of beads P, where the exact results are obtained only in the limit of $P \to \infty$. When the temperature T is decreased, the number of beads in the PIMC calculation must be increased according to $P \approx 1/T$ in order to maintain the same error. This further increases the complexity of the system, which is complex enough even before taking into account the NQEs. The numerical convergence of the Monte Carlo calculation is hampered by the sampling problems associated with the rugged character of the cluster's PES. More specifically, the complexity increases exponentially with the system size N if measured in terms of the number of physically relevant local energy minima that have to be sampled. In some well-documented cases, the existence of just two basins of attraction (funnels) separated by a high energy barrier is sufficient to make the numerical problem unfeasible, even when using advanced sampling techniques (see ref 27 for examples). This so-called "broken ergodicity" problem is often not appreciated and/or simply ignored, perhaps due to the lack of a universal solution. A single Monte Carlo simulation performed on such a system may seem converged, while in reality, the results could drastically change if a different initial condition is used. This is important, since a Monte Carlo simulation is naturally initialized using the global potential energy minimum, unless multiple independent simulations are carried out. Moreover, when the choice of the initial condition is not specified explicitly, it is safe to assume that this is the default. As mentioned earlier and also demonstrated below, the global energy minimum often contributes very little or not at all to the ground state wavefunction for a quantum cluster, which makes the "natural choice" for the initial conditions become another source of systematic errors.

Early DMC studies by Guardiola and Navarro[11,12] using a version of DMC with importance sampling (DMC-IS) have

https://dx.doi.org/10.1021/acs.jpca.0c07107
J. Phys. Chem. A 2020, 124, 8766−8777

shown essentially smooth chemical potential curves with increasing cluster size, with the exception of a prominent minimum at $N = 13$ (see Figure 1). While these results seem reasonable and the existence of a prominent minimum at $N = 13$ is expected, numerically they may be questionable, particularly for sizes $N \geq 30$. In fact, these authors used very small random walker populations ($N_w \approx 10^3$), while their numerical tests (changing N_w in the range of 500−2000) showed a ∼2 K bias for E_{30}. Although they assumed that the bias was a smooth function of N, no evidence for this claim was provided, and to the best of our knowledge, no follow-up of this study has appeared in the literature.

Later, Sola and Boronat[13] also applied DMC-IS to $(pH_2)_N$ for a broader size range, $N = 13$−75. Unlike the previous DMC-IS results,[11,12] they reported zigzagged shapes for the chemical potential μ_N (see Figure 1). In addition, these authors claimed that they were able to establish the alternating (in N) behavior between the liquid and solid phases for the ground state of $(pH_2)_N$ clusters. However, these results are hardly reliable. First, the authors used a less accurate importance sampling (IS) wavefunction Ψ_T than that in ref 12. Second, they did not report any convergence studies for their DMC-IS calculations. Specifically, they neither provided the ground state energy estimates E_N as a function of N_w nor did they specify the values of N_w used. Third, in order to enforce the "solid" state of the cluster, they used an IS wavefunction Ψ_T localized around its global energy minimum. As aforementioned, this choice is often wrong for hydrogen clusters because of the strong quantum effects. Moreover, even when the wavefunction is localized in an energy minimum, the center of localization must be shifted relative to the classical equilibrium configuration due to the asymmetry of the potential energy well.[7] This means that an unshifted solid IS wavefunction is always inadequate.

The population size bias in DMC-IS was investigated by Boninsegni and Moroni.[21] For this study they considered the $(pH_2)_{48}$ cluster, which they referred to as "a simple test system." Consequently, the energy, E_{48}, computed by DMC did not show any sign of convergence when N_w was as large as 2×10^5, i.e., by about two orders of magnitude larger than in the previous DMC-IS calculations.[11−13] Our own convergence tests (see below) show that even for much smaller systems (e.g., $(pH_2)_{26}$) the population size bias in DMC-IS eventually vanishes but only at values of $N_w \approx 5 \times 10^5$. Moreover, before it vanishes completely for E_N, the systematic errors in DMC-IS do not cancel for the chemical potential $\mu_N = E_N - E_{N-1}$. To make matters worse, there is still an uncertainty in the validity of the "converged" chemical potentials and other observables, even when the results do converge with respect to N_w. This is because of the uncontrollable bias introduced by the particular choice of the IS wavefunction Ψ_T. This bias has no systematic solution since the quality of the IS wavefunction typically obtained by the variational Monte Carlo (VMC) method is limited to relatively simple forms.

In addition to DMC studies, a number of PIMC (finite T)[9,15,19,22,28−30] and PIGS ($T = 0$ K)[16,17,23] calculations on pure *para*-hydrogen (i.e., excluding pure *ortho*-deuterium and *ortho*-deuterium-doped clusters) have been reported in the past few decades.

Reference 19 used PIMC to compute the superfluid fractions ρ_s in $(pH_2)_N$ clusters ($N = 10$−40), which appeared to be size-sensitive. For example, for the $N = 26$ cluster they found a significant drop of ρ_s relative to $N = 25$ and 27. This was explained by the behavior of the corresponding radial correlation functions $\rho(r)$, where r defines the distance from pH_2 molecules to the cluster's center of mass. Here and throughout the paper, we will consider the quantity $\rho(r)r^2$, which is normalized as

$$\int_0^\infty \rho(r)r^2 \, dr = N \tag{1}$$

so that the weight of each peak is equal to the number of particles forming the corresponding spherical layer. The radial distributions for $N = 25$, 26, and 27 computed by either PIMC or PIGS were later reproduced in a number of publications.[15,23,29,30] In Figure 2 we show an example from a recent

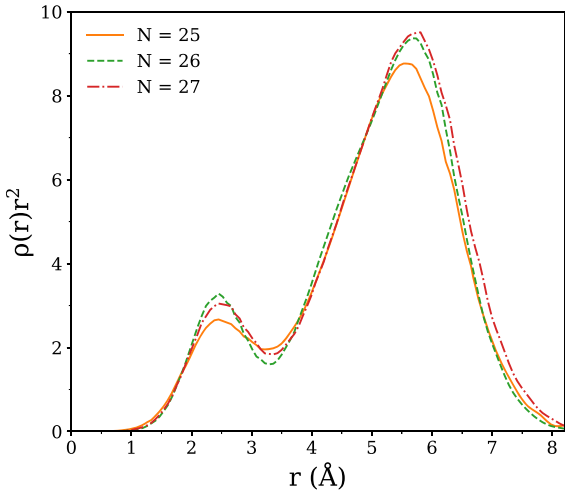

Figure 2. Radial distributions $\rho(r)r^2$ (with respect to the cluster's center of mass) from ref 23 computed by VPI (a variant of PIGS) for $(pH_2)_N$ clusters with $N = 25$, 26, and 27. The appearance of the first peak for $N = 26$ was used in a number of publications[15,23,29,30] as evidence for the more solid-like ("magic") character of this cluster.

paper by Miura.[23] At first glance, there seems to be a structural change when going from $N = 25$ to 26 with the peak at $r \approx 1.6$ Å becoming noticeably sharper. This was interpreted by all of the aforementioned authors as structural evidence for the inner shell, which is apparently a tetrahedron formed by four pH_2 molecules, being more solid-like (i.e., less delocalized) for $N = 26$ compared to the other two clusters. That is, the $N = 26$ cluster is more "solid" than its neighbors (i.e., $N = 25$, 27), and as such, it was unanimously labeled as a magic number cluster. (Reference 29 goes even further by plotting a 3D image of $(pH_2)_{26}$ in which each pH_2 molecule is localized in space.) We note, however, that the structural evidence based on the appearance of $\rho(r)$ mentioned in all the above references is rather coincidental. This is because the peak widths in $\rho(r)$ are very sensitive to where the "cluster's center" is assumed to be. In fact, the position of the cluster's center of mass is generally shifted with respect to the actual center of the shells, and consequently, the peaks become broader when this shift is larger. Below, we show that placing the center at that of the inner shell removes the qualitative differences between radial distributions of these clusters. The fact that the radial distribution is so sensitive to the choice of the center makes it inconvenient for structural analysis. In fact, much better quantities exist, such as the pair correlation function $g(r)$ or the orientational bond order parameters,[31] Q_4 and Q_6.

https://dx.doi.org/10.1021/acs.jpca.0c07107
J. Phys. Chem. A 2020, 124, 8766−8777

For the chemical potential μ_N, the PIMC results at T = 1 K from ref 29 agree with the DMC results of Guardiola and Navarro[12] for small sizes N but start to show erratic behavior for N > 17, with the disagreement growing with N. This disagreement becomes as large as 30% of the chemical potential itself at N = 32. Furthermore, at a lower temperature (T = 0.25 K), the disagreement between PIMC and DMC is much smaller but still noticeable. In order to rationalize the strange increase in size sensitivity when the temperature was increased, the authors suggested that strong quantum delocalization ("quantum melting") only takes place at sufficiently low temperatures (e.g., T = 0.25 K), while at higher temperatures (e.g., T = 1 K), these clusters become solid-like and essentially resemble the classical behavior. Similar conclusions were reached in refs 9, 15, exclusively based on examining the behavior of $\rho(r)$ as a function of temperature. We note that all of the mentioned PIMC calculations were performed by taking into account the nuclear exchange. At the same time, the authors of refs 9, 15 stated and showed some numerical evidence that the structural properties (such as $\rho(r)$) are hardly affected by Bose statistics. This conclusion, i.e., that due to the NQEs a pH_2 cluster undergoes a liquid−solid transition with increasing (not decreasing!) temperature, solely made from observing the behavior of the radial correlation function $\rho(r)$, seems very intriguing but also very controversial. Surprisingly, to the best of our knowledge, it has not been revisited in the literature. Despite being disconcerted by this conclusion, we are not in the position of questioning it any further, as this goes beyond the scope of the present paper.

Another study investigating the ground states of $(pH_2)_N$ clusters (N = 2−55) using the PIGS method was carried out by Cuervo and Roy.[16,17] Unlike the smooth DMC-IS chemical potential curves reported around the same time by Guardiola and Navarro,[11,12] their μ_N dependence showed strong size sensitivity for $N \geq 26$ (see Figure 1). As a result, they suggested several new magic number clusters (starting with N = 26). In order to rationalize their findings, they also used the radial distribution $\rho(r)$. The striking qualitative disagreement between DMC and PIGS was inspiring and seems to be unsettled until now. For example, in a recent paper, Miura[23] used the variational Path Integral (VPI) method (which is essentially a variant of PIGS) to study the ground states of $(pH_2)_N$ clusters for N = 3−40. Qualitatively the VPI results (see Figure 1) are consistent with those from PIGS[17] and PIMC (T = 0.5 K)[15] in that the μ_N curve also displays a zigzagged behavior for $N \geq 26$. However, there were still some substantial quantitative discrepancies in the actual values of μ_N between the three sets of data. Miura[23] also used $\rho(r)$ for structural analysis but additionally performed inherent structure analysis for N = 26, which showed several isomers sampled during the simulation period. In spite of this observation, the author still concluded that the N = 26 cluster is more rigid than N = 25 and 27 for which the inherent structure analysis was not presented.

Finally, a thorough DMC study of just two systems, $(pH_2)_{19}$ and $(pH_2)_{38}$, and their deuterium isotopologues, was reported by one of us.[14] Rather than trying to directly settle the magic number controversy, this study focused on the structural analysis as a function of quantum strength (deuterium versus hydrogen). The main tool for this study was the inherent structure analysis in which the random walker population was quenched to determine the isomer fractions (see below). This analysis on both pH_2 clusters resulted in millions of inherent structures representing all existing symmetry motifs that were supported by the underlying PES, thereby leaving no doubt about the high level of disorder of the ground state wavefunction. We believe that this finding alone can serve as an indirect indication of the lack of size sensitivity of the $(pH_2)_N$ clusters, while exposing the sheer complexity of these clusters that has certainly been underappreciated in the field.

In accordance with the above discussion, we will focus on the smallest, yet still interesting, size range (N = 24−28), since the discrepancy between methods (e.g., DMC and PIGS) become apparent at N = 26. We do so in order to demonstrate that these clusters are size insensitive, and hence, there is no evidence for calling $(pH_2)_{26}$ a magic number cluster. In addition, we will address some numerical issues associated with the DMC calculations, where in particular, we will investigate the performance of DMC with and without IS.

METHODS

The present DMC calculations without IS as originally formulated by Anderson,[32,33] were carried out following ref 14, while the DMC calculations with importance sampling (DMC-IS) were implemented following refs 11, 13. All calculations here were done using the SG potential.[3]

To briefly summarize the method, we employed the variant of DMC that uses a population of N_w random walkers with equivalent weights that sample the configuration space bounded by the PES, which collectively represent the system wavefunction at projection time τ. At each time step of length $\Delta\tau$, a "branching procedure" is introduced in which some random walkers are replicated and some are killed to keep the random walker population virtually constant and, hence, to stabilize the average estimate of the ground state energy $\langle E_{ref}\rangle$. At sufficiently long τ, the ensemble of random walkers approaches a stationary distribution and the instantaneous energy $E_{ref}(\tau)$ fluctuates in a predictable way around its average value $\langle E_{ref}\rangle$, and the time average provides as estimate of the ground state energy:

$$E_0 \approx \frac{1}{\tau_{max}} \int_0^{\tau_{max}} E_{ref}(\tau)\, d\tau \tag{2}$$

In the limit of $\Delta\tau \to 0$, $N_w \to \infty$, and the total propagation time $\tau_{max} \to \infty$, the random walker distribution converges to the exact ground state wavefunction with $\langle E_{ref}\rangle = E_0$, i.e., the exact ground state energy.

Here, the error bars for the energies are calculated using a reblocking scheme in which standard deviations are calculated from the variance of interval averages following an equlibration period.[34]

DMC-IS follows a similar methodology except with an additional constraint imposed on the random walker population through the IS wavefunction $\Psi_T(r)$. More specifically, the Schrödinger equation is rewritten in terms of a new wavefunction

$$f(r, t) = \Psi_T(r)\, \Psi(r, t) \tag{3}$$

which satisfies the diffusion equation with a drift term that depends on Ψ_T. This acts as an external force to guide the diffusion of random walkers across the configuration space. Here, we use the most simple IS wavefunction that includes only two-body terms

https://dx.doi.org/10.1021/acs.jpca.0c07107
J. Phys. Chem. A 2020, 124, 8766−8777

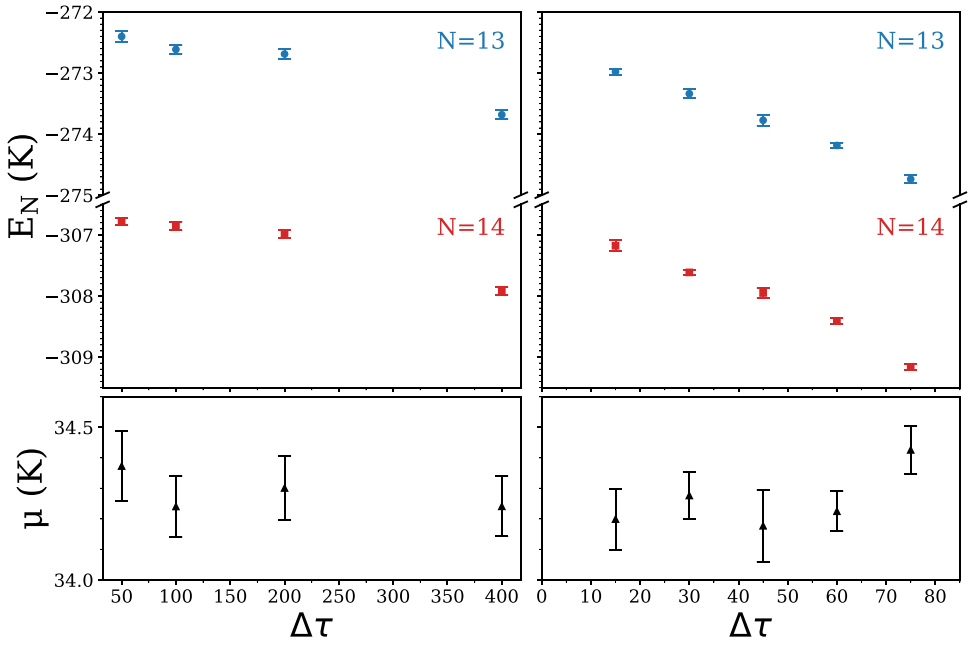

Figure 3. DMC (left) and DMC-IS (right) energy estimates (K) for clusters E_{13} and E_{14} and the chemical potential $\mu_{13} = E_{14} - E_{13}$ as a function of time step $\Delta\tau$ using $N_w = 5 \times 10^6$ and $\tau_{max} = 2 \times 10^7$ au, and $N_w = 5000$ and $\tau_{max} = 10^7$ au, respectively.

$$\Psi_T(r) = \exp\left(-\sum_{i>j} u(r_{ij})\right); \; u(r) = \frac{1}{2}\left(\frac{r}{b}\right)^5 + \frac{\beta r}{N} \tag{4}$$

where r_{ij} defines the pair distances between pH_2 molecules. This was implemented in the previous aforementioned studies (see, e.g., refs 11, 13). The constants b and β are obtained by the VMC method by minimizing the following energy functional:

$$E(b;\beta) = \frac{\langle \Psi_T|\hat{H}|\Psi_T\rangle}{\langle \Psi_T|\Psi_T\rangle} \tag{5}$$

The exact values for these parameters vary slightly with N. However, since this IS wavefunction is far from the exact ground state wavefunction regardless of whether the best parameters are used, for convenience, we implemented the size-independent values[13] b = 3.58 Å, β = 2.79 Å^{-1}, unless specified otherwise.

Besides the ground state energies, we also compute the following structural properties:

(i) The orientational bond order parameters, Q_4 and Q_6.[31]

(ii) The radial correlation function $\rho(r)$ with respect to the cluster's center (to be specified later).

(iii) The pair correlation function $g(r)$, where the quantity $g(r)r^2$ normalized as

$$\int_0^\infty g(r)r^2 \, dr = 1 \tag{6}$$

will be plotted for consistency.

(iv) The isomer fractions f_k ($\sum_k f_k = 1$) obtained by quenching the random walker configurations during the DMC calculation. The quenching is done using the conjugate gradient method. For each isomer, f_k is set to be proportional to the number of configurations minimized upon quenching into the corresponding potential energy minimum.

The use of IS comes with great benefits in terms of reducing statistical errors and, most importantly, converging DMC-IS energies and other observables at relatively small values of N_w (i.e., small compared to those needed in the case of DMC). This, however, comes with a price. Theoretically, the numerically converged (with respect to N_w, $\Delta\tau$, and τ_{max}) DMC-IS results should not depend on the IS wavefunction Ψ_T. However, the seemingly converged results do depend on Ψ_T in practice, and this dependence is hard to keep under control because the systematic improvement of Ψ_T is limited to relatively simple forms. This in turn makes the problem of assessing the accuracy, particularly of the chemical potential estimates, orders of magnitude more difficult than merely getting the results. In this paper, we will only demonstrate that a nontrivial bias associated with the choice of Ψ_T exists since a systematic investigation of such a bias would be too costly and is beyond the scope of this paper.

It is also important to point out that observables of operators (e.g., assuming a function of the coordinate $A(\mathbf{r})$), such as

$$\langle A\rangle := \frac{\int |\Psi(r)|^2 A(r) \, dr}{\int |\Psi(r)|^2 \, dr} \tag{7}$$

that do not commute with the system's Hamiltonian, cannot be computed naturally within the standard DMC framework. This leaves the ground state energy as essentially the only both interesting and true physical observable that can be computed in a straightforward manner. However, the structural properties defined by the system's wavefunction $\Psi(\mathbf{r})$ can still be characterized using the quantities that are easily computed within the DMC framework. The most natural is the Ψ-averaged quantity

$$\langle A\rangle_1 := \frac{\int A(r)\,\Psi(r) \, dr}{\int \Psi(r) \, dr} \tag{8}$$

which is computed by averaging over both the random walker population and time τ. Although not true physical observable, this can still provide insight into the ground state properties (e.g., the structural properties) and be related to the true, i.e.,

https://dx.doi.org/10.1021/acs.jpca.0c07107
J. Phys. Chem. A 2020, 124, 8766−8777

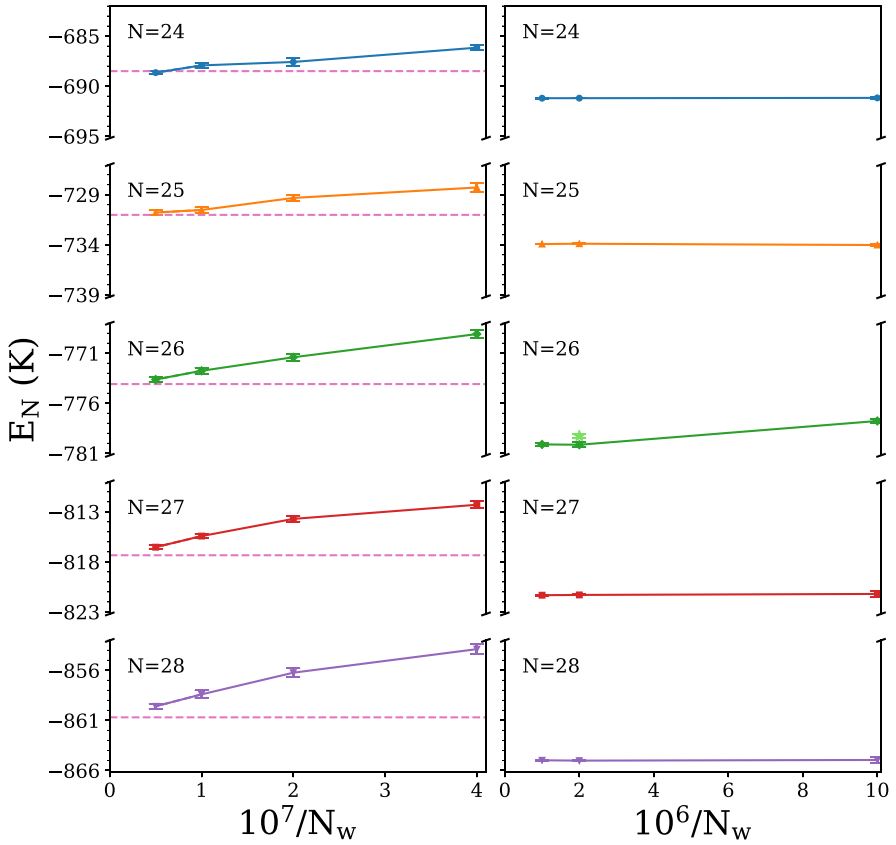

Figure 4. DMC energy estimates (K) of $(pH_2)_N$ clusters with sizes N = 24−28 using $\Delta\tau$ = 200 au (left) and from DMC-IS using $\Delta\tau$ = 30 au (right). All calculations were run with $\tau_{max} = 2 \times 10^7$ au. The DMC-IS energy for N = 26 using better optimized parameters for the IS wavefunction (b = 3.65 Å and β = 2.06 Å^{-1}) is also shown for $N_w = 5 \times 10^5$ (green star). The dashed horizontal lines show the DMC-IS results from ref 12 using a better IS wavefunction.

Ψ^2-averaged, physical observable (eq 7). Meanwhile, one can naturally estimate both the Ψ-averaged observable

$$\langle A \rangle_1 = \frac{\int f(\mathbf{r})\, A(\mathbf{r})/\Psi_T(\mathbf{r})\, d\mathbf{r}}{\int f(\mathbf{r})/\Psi_T(\mathbf{r})\, d\mathbf{r}} \tag{9}$$

and the true physical observable through the so-called "mixed estimate"

$$\langle A \rangle \approx \langle A \rangle_{IS} = \frac{\int \Psi(\mathbf{r})\, \Psi_T(\mathbf{r})\, A(\mathbf{r})\, d\mathbf{r}}{\int \Psi(\mathbf{r})\, \Psi_T(\mathbf{r})\, d\mathbf{r}} = \frac{\int f(\mathbf{r})\, A(\mathbf{r})\, d\mathbf{r}}{\int f(\mathbf{r})\, d\mathbf{r}} \tag{10}$$

using DMC-IS. The problem with eq 10 is that it depends entirely on the quality of the IS wavefunction, which for a complex many-body system, is never good enough and thereby introduces an uncontrollable bias.

RESULTS AND DISCUSSION

The Ground State Energies and Chemical Potential. The finite values of N_w and $\Delta\tau$ are sources of systematic errors in both DMC and DMC-IS. Figure 3 shows the energy estimates, E_{13} and E_{14}, as a function of $\Delta\tau$ computed using DMC and DMC-IS. As shown, the $\Delta\tau$ bias is much stronger when IS is used, which can be explained by the presence of the drift term in the diffusion equation associated with DMC-IS. Notably however, there is a good cancellation of the $\Delta\tau$ bias for chemical potential $\mu_{13} = E_{14} - E_{13}$. Based on these results, all of the following calculations were performed using $\Delta\tau$ = 200 au for DMC and $\Delta\tau$ = 30 au for DMC-IS, which result in systematic errors (for μ_N) well within the statistical errors. Another important point to highlight here is that the results from DMC and DMC-IS coincide if extrapolated to the limit of $\Delta\tau \to 0$. We will show below that this is in fact not the case for larger cluster sizes, where we observe the manifestation of the "curse of dimensionality" in both DMC and DMC-IS calculations.

Next, we present the results for the size range N = 24−28 from DMC and DMC-IS calculations. Figure 4 shows the energy estimates E_N as a function of population size N_w. One can see that the bias for the unguided DMC energies remains at population sizes as large as $N_w \approx 10^7$. At the same time, the DMC-IS energies stop changing around $N_w = 5 \times 10^5$, and the two sets of energy estimates disagree by about 5 K. Notably, the results from the unguided DMC calculation using the largest population size ($N_w = 2 \times 10^7$) agree within ∼1 K with DMC-IS results from ref 12 with the discrepancy growing with N. (Note, again, that ref 12 used a much better IS wavefunction Ψ_T which included three-body terms.) Although this figure only confirms the results reported a decade ago by Guardiola and Navarro,[12] it also emphasizes the dangers associated with using IS. One can see that the present DMC-IS energies using the less accurate two-body IS wavefunction are strongly biased with the systematic errors undetectable without a comparison to accurate results. It should also be noted that this bias is too large to be due to the finite value of $\Delta\tau$, which is estimated to be less than 1 K.

These comparisons are further highlighted in Figure 5, which shows the chemical potential curves μ_N obtained from

https://dx.doi.org/10.1021/acs.jpca.0c07107
J. Phys. Chem. A 2020, 124, 8766−8777

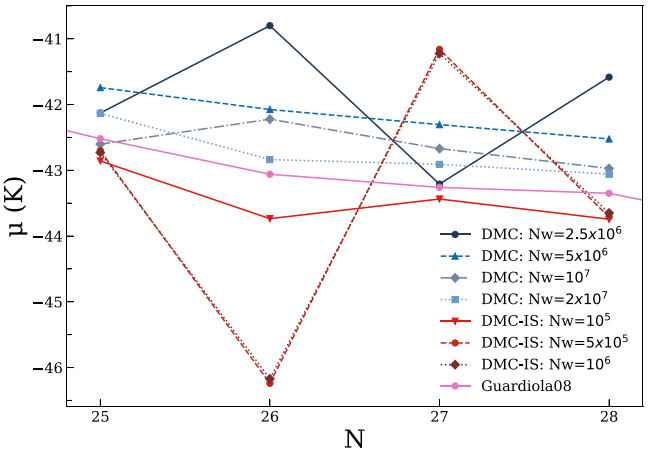

Figure 5. Chemical potential curves $\mu_N = E_{N-1} - E_N$ generated from the data in Figure 4.

the data presented in Figure 4. The chemical potential curve computed by DMC becomes relatively smooth as N_w increases in the calculations without IS. On the other hand, the present "converged" (with respect to N_w) DMC-IS results show zigzagged chemical potential curves with a minimum at N = 26. It is very likely, albeit difficult to claim with 100% certainty, that the observed size sensitivity in the present DMC-IS result is simply an artifact of the bias introduced by the particular choice of the IS wavefunction in the form of equation eq 4.

To conclude this subsection, there is no convincing energetic data that points to the existence of a "magic number" cluster in this range. In addition, the present results further highlight the challenging nature of these calculations that has led to the lack of consensus regarding the values of the exact energies and chemical potential. To this end, we now turn to the analysis of structural properties of the ground state wavefunctions, which will provide more insight into the issue of size sensitivity in these systems.

The Structural Analysis. While the accuracy of the energy estimates appear to be very sensitive to numerical details using any of the in-principle-exact methods (PIMC, PIGS, DMC, DMC-IS), the structural properties appear to be much more robust. As an example, Figure 6 shows the radial distribution $\rho(r)$ and the pair correlation function $g(r)$ for $(pH_2)_{26}$ computed using unguided DMC with various populations of random walkers N_w. Even for the relatively small population size of $N_w = 2.5 \times 10^6$, for which there is a significant bias in the energy estimate, the spatial distributions are well converged. Furthermore, these results are unchanged with respect to the time step $\Delta\tau$, and the distributions remain within the line width in the graph (not shown). Similar results are obtained in the case of DMC-IS (not shown).

As we have seen already, there is a clear bias associated with the use of the trial wavefunction in the form of eq 4. That is, the choice of the trial wavefunction Ψ_T matters, in spite of the fact that DMC-IS is an in-principle-exact method, and in the limit of $N_w \to \infty$, $\Delta\tau \to 0$, $\tau \to \infty$, it should provide the exact results regardless of what Ψ_T is. Once again, IS can significantly reduce statistical errors and improve convergence with respect to N_w. It does so by guiding the random walkers away from the parts of the configuration space not represented by Ψ_T, thus reducing the effective volume of the sampling region accordingly. Moreover, such a reduction scales exponentially with the system size N. However, the IS procedure can simultaneously omit some relevant information about the system in regions where Ψ_T does not have appreciable overlap with the wavefunction. Unfortunately, this bias is impossible to assess without having access to accurate results obtained by other methods. To this end, we turn to Figure 7, which further adds to the evidence indicating that DMC-IS is biased.

The discrepancy between the converged distributions (with respect to a given method) of $\rho(r)$ and $g(r)$ computed with DMC versus DMC-IS is evident in Figure 7. One can see that this discrepancy is much greater than the statistical errors. Moreover, when the variational parameters, b and β (*cf.* eq 4)), are adjusted slightly for N = 26, the distributions also change. Therefore, once again, we observe structural characteristics that are indicative of a bias introduced as a result of using IS. This structural difference, which may seem relatively small at first glance, can correspond to greater differences in the ground state wavefunctions. This is reflected in the bias observed in the DMC-IS energies in Figure 4.

It should be reiterated that the Ψ-averaged quantities (*cf.* eq 8) are naturally obtained within the DMC framework, while both the Ψ-averaged observables and the mixed estimate 10 of the Ψ^2-averaged quantities (i.e., the true physical observables), are naturally calculated within the DMC-IS framework. To allow one to ascertain the validity of this Ψ-averaged quantity as a measure to investigate structural properties, we addition-

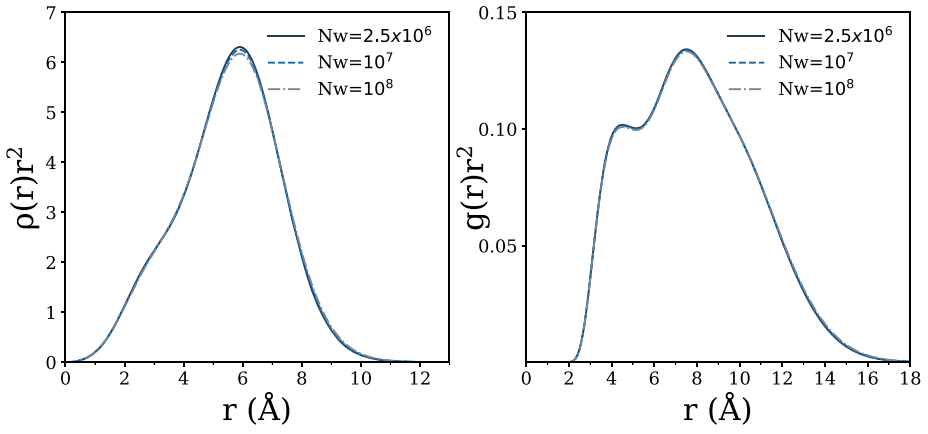

Figure 6. Ψ-averaged radial distribution $\rho(r)r^2$ (with respect to the cluster's center of mass) and the pair correlation function $g(r)r^2$ for $(pH_2)_{26}$ using different random walker populations N_w computed by DMC.

https://dx.doi.org/10.1021/acs.jpca.0c07107
J. Phys. Chem. A 2020, 124, 8766−8777

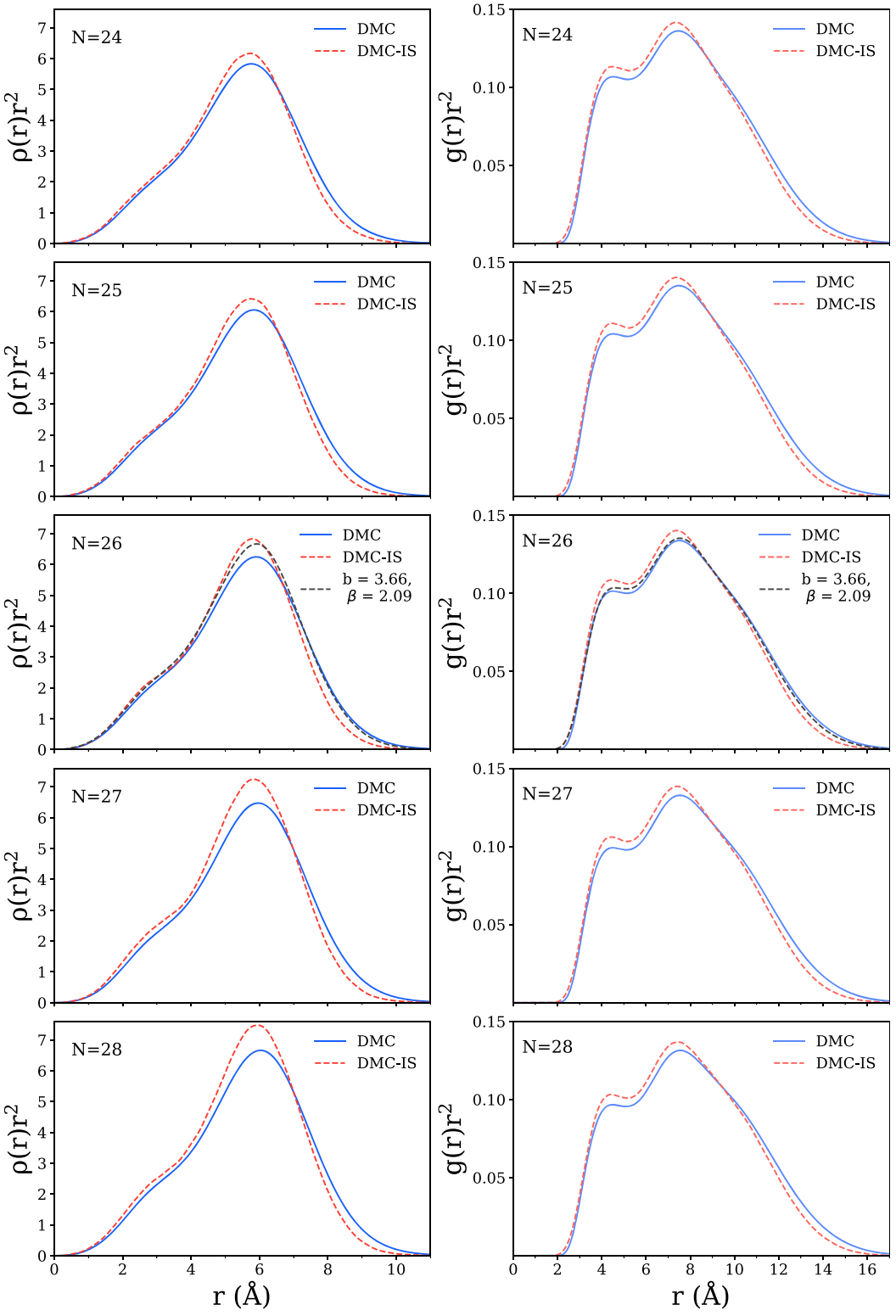

Figure 7. Ψ-averaged radial distribution $\rho(r)r^2$ (with respect to the cluster's center of mass) and the pair correlation function $g(r)r^2$ computed with DMC using $N_w = 10^7$ as well as the Ψ-averaged quantities from DMC-IS using $N_w = 5 \times 10^5$ for $N = 24-28$. Results with different IS parameters; b = 3.65 Å and β = 2.06 Å^{-1} for $N = 26$ is also shown.

ally show both Ψ and Ψ^2-averaged distributions for $N = 26$, computed using DMC-IS in Figure 8. As expected, Ψ^2-averaged distributions are more structured than the Ψ-averaged quantities. Nonetheless, one can still observe the utility of using these strictly speaking unphysical (Ψ-averaged) quantities to characterize a cluster's structure. Furthermore, for the purpose of this work, which is to investigate size sensitivity and to evaluate the DMC methods, the distinctions between these distributions are inconsequential.

In order to relate the present results with those reported in the literature, we compare some of them with the best we have, i.e., the mixed estimates of the radial distributions $\rho(r)$, in

https://dx.doi.org/10.1021/acs.jpca.0c07107
J. Phys. Chem. A 2020, 124, 8766−8777

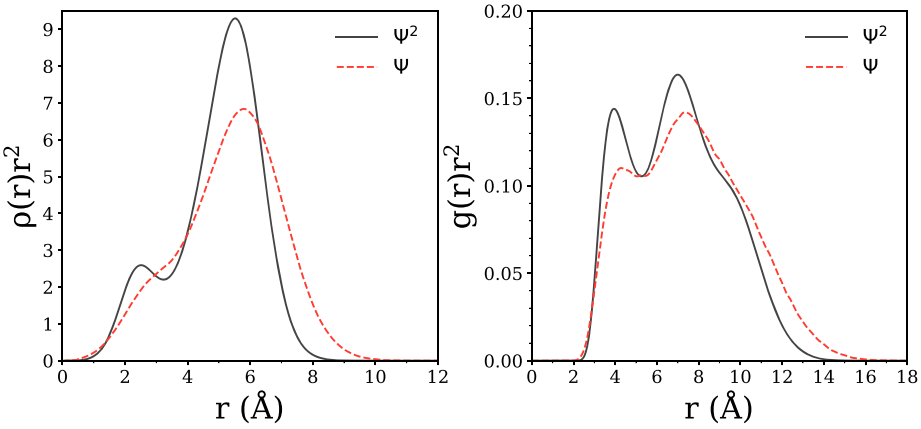

Figure 8. Ψ- and Ψ^2-averaged radial distributions $\rho(r)r^2$ (with respect to the cluster's center of mass) and the pair correlation functions $g(r)r^2$ calculated using DMC-IS for $(pH_2)_{26}$ using $N_w = 5 \times 10^5$.

Figure 9. While the latter is an approximation by construction, to our surprise, we find significant discrepancies between the results obtained using in-principle-exact methods (PIGS, VPI and PIMC), which indicates that at least some of them are not well converged.

We now turn to one of our motivations for studying these clusters, which is to investigate the quantum delocalization and size sensitivity using structural analysis of the ground state wavefunctions for which the DMC method is most suited. The left panels in Figure 10 show the isomer fractions as a function of the isomer energies, i.e., the potential energy values at the corresponding minima of the PES. These were obtained by quenching the random walker configurations during the DMC runs. First of all, we note that for each cluster, the ground state wavefunction is delocalized over a very large number of isomers (i.e., potential energy minima), with individual isomers contributing less than 4% to the wavefunction. (However, in order to make the figure readable, we only display a section that corresponds to $f_k > 0.0002$.) The fact that there is no particular cluster configuration that could be associated with the structure of the ground state, e.g., for $N = 26$, makes the speculations about its solid-like character[15,23,29,30] at least questionable. Second, in all cases, except maybe $N = 27$, the most contributing isomer is not the global energy minimum. The right panels in Figure 10 show the same isomer fractions but as a function of the Q_6 orientational bond order parameter. This plot demonstrates that the wavefunction is delocalized over a large region of the configuration space and represents all symmetry motifs that are supported by the underlying PES. (Here, the reader is referred to ref 35 in which the structural analysis of Lennard−Jones clusters using Q_6 is carried out.)

We now remind the reader of the ill-defined nature of the radial distribution $\rho(r)$ when the distance r is measured between the pH_2 molecules and the cluster's center of mass. In order to demonstrate this point, we show Ψ-averaged $\rho(r)$ computed using a single configuration of the most populated isomer for each cluster in the range $N = 24$−28 (see the top panel of Figure 11). This is done by averaging $\rho(r)$ over the harmonic ground state wavefunction for the corresponding potential energy minimum. If one assumes that such distribution is a unique characteristic of a cluster's structure, then this plot would indicate a high level of size sensitivity in these clusters. However, in the middle panel of Figure 11, we show that this is in fact not true. We notice that in all cases, the inner shell is formed by four particles, and hence this panel

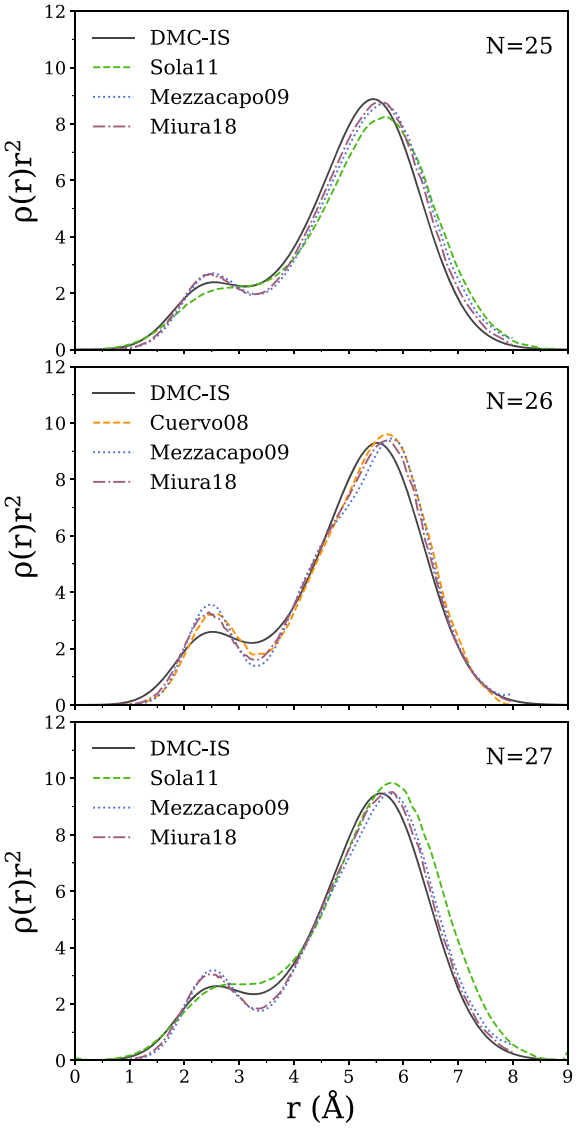

Figure 9. Mixed estimates of the radial distributions $\rho(r)r^2$ (with respect to the cluster's center of mass) computed by DMC-IS using $N_w = 5 \times 10^5$ for $N = 25$−28 compared to those reported in various publications: Sola11 (ref 17, using PIGS), Miura18 (ref 23, using VPI, a variant of PIGS), and Mezzacapo09 (ref 29, using PIMC, $T = 0.5$ K).

https://dx.doi.org/10.1021/acs.jpca.0c07107
J. Phys. Chem. A 2020, 124, 8766−8777

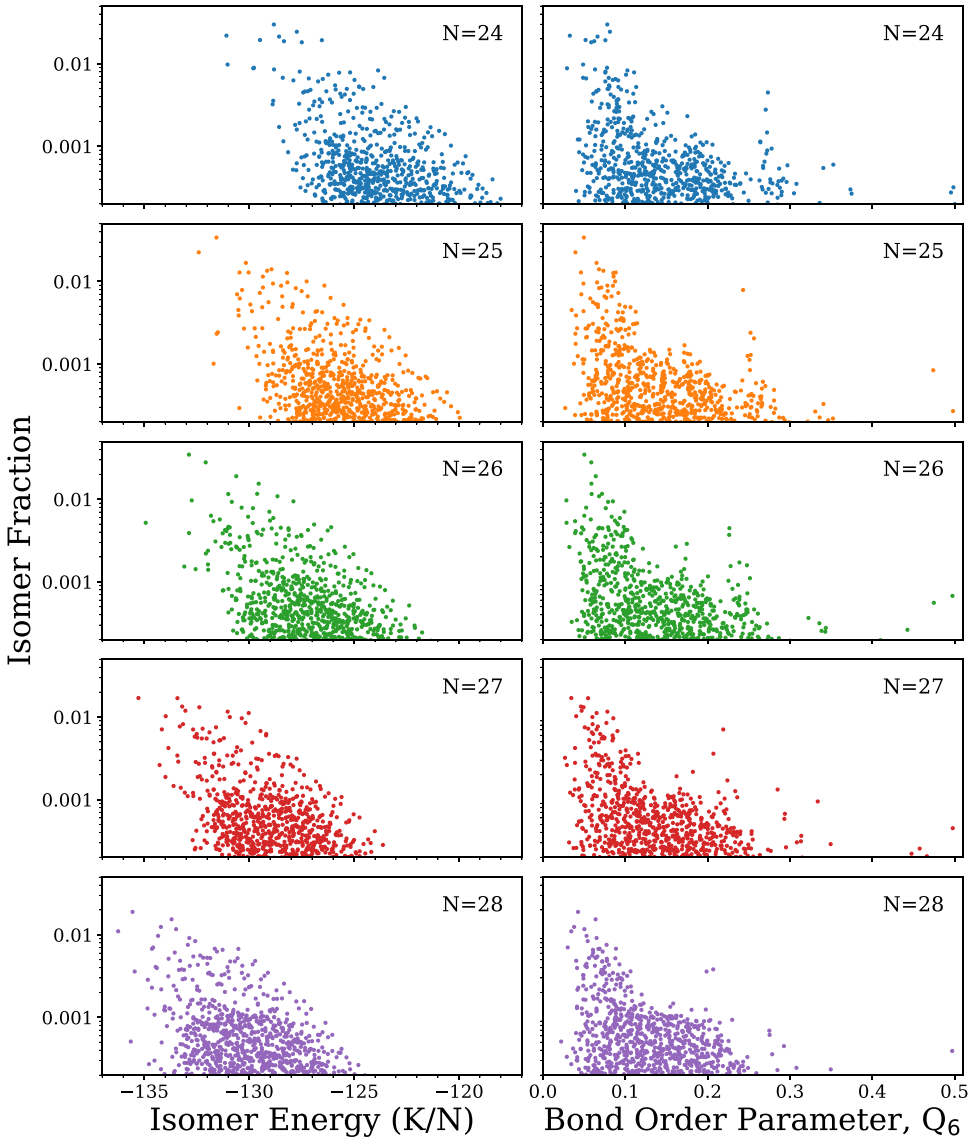

Figure 10. Isomer fraction f_k from the DMC simulations (using $N_w = 2 \times 10^7$) for $N = 24–28$ as a function of isomer energy per molecule (left) and as a function of the orientational bond order parameter, Q_6 (right). (Note the logarithm scale.) While for all the observed isomers $f_k < 0.04$, only isomers for which $f_k > 0.0002$ are shown.

shows that the distributions based on distances measured with respect to the center of mass of the inner shell is a more appropriate definition of $\rho(r)$. Strikingly, all five radial distributions look nearly identical around the first peak and resemble the radial distribution function of a perfect tetrahedron. Meanwhile, the second peak gradually increases in size with the increasing number of particles in the second shell. The bottom panel in Figure 11 shows the pair correlation function $g(r)$, which confirms that all five isomers are structurally very similar. We note here that other highly populated isomers from Figure 10 result in similar distributions (not shown). Finally, Figure 12 shows the Ψ-averaged radial distributions and pair correlation functions from the DMC calculations for $N = 24–28$. These plots most clearly confirm the conclusion that structurally all clusters in the range $N = 24–28$ are the same, as both distributions change systematically with increasing cluster size.

CONCLUSIONS

In this paper, we revisited *para*-hydrogen clusters, which have been the focus in numerous publications. The controversial issue that we tried to address was whether the size sensitivity in these clusters persists when the strong quantum effects are taken into account. The magic number clusters are observed in atomic and molecular clusters of various kinds, and the phenomenon seems to be generic. Indeed, all classical (i.e., without NQEs) clusters of particles interacting via a short-range potential display high size sensitivity. For example, given the number N of constituents in a cluster, its global energy minimum usually corresponds to the structure of high symmetry in which the number of nearest-neighbor pairs is maximized, and hence, the total energy is minimized. Clearly, there are always specific sizes with perfect symmetries for which the binding energy per one constituent is maximized compared to its neighbors (i.e., the sizes corresponding to a spike in the chemical potential μ_N). It is also apparent that smaller spikes in the μ_N dependence should exist as well. Again,

https://dx.doi.org/10.1021/acs.jpca.0c07107
J. Phys. Chem. A 2020, 124, 8766−8777

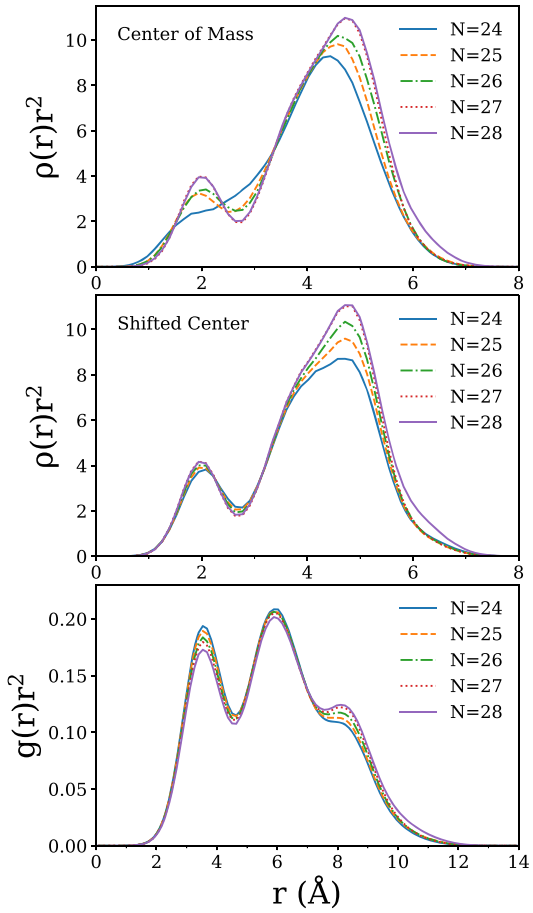

Figure 11. Top panel: Ψ-averaged radial distributions $\rho(r)r^2$ with respect to the cluster's center of mass, which was computed by averaging over the harmonic ground state wavefunctions of the most populated isomers for N = 24−28. Middle panel: Same as the top panel but the center is set to coinside with the center of the inner shell of the cluster. Bottom panel: The pair correlation functions $g(r)r^2$, but otherwise the same as the other two panels.

this is the general property of systems with short-range potentials. At the same time, the situation becomes more complicated when the range (i.e., the ratio between the effective width of the attractive well of the pair potential and the minimum distance) of the interacting pair potential between the constituents in the cluster becomes sufficiently large,[36] as in this case where the total energy of the cluster is determined by the overall shape of the cluster rather than the number of the nearest neighbor pairs. Consequently, for long-range potentials, the symmetry is no longer a factor in determining the cluster's energetics, which in turn leads to disordered (liquid-like) structures. Since magic number patterns are closely related to the presence of symmetries, the lack of the latter implies the lack of the former. Interestingly, the increase of quantum strength in a many-body system (such as that measured in terms of de Boer quantum delocalization length Λ in Lennard-Jones clusters) leads to an increase in the effective range of the potential.[7] That is, strong NQEs result in disordered structures and hence a loss of size sensitivity. References 10, 14 together with the present results strongly suggest that this is the case for *para*-hydrogen clusters.

As we have demonstrated in this paper, the lack of size sensitivity can be confirmed using adequate structural markers

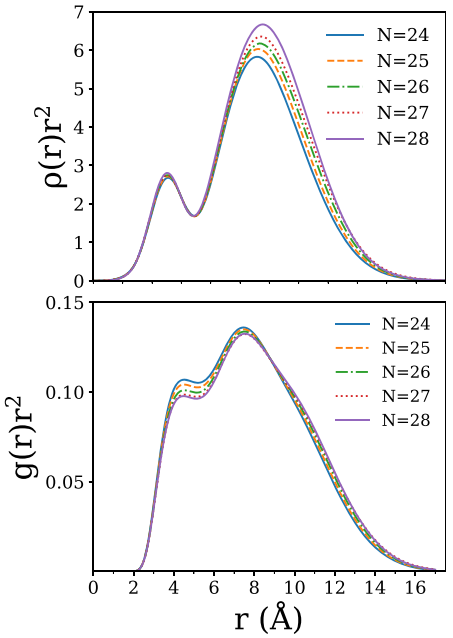

Figure 12. Ψ-averaged radial distributions $\rho(r)r^2$ (with respect to the center of the inner shell of the cluster) and the pair correlation functions $g(r)r^2$ for N = 24−28 from DMC calculations using $N_w = 2 \times 10^7$.

to characterize and compare the $(pH_2)_N$ clusters of different sizes. Another interesting observation made in this paper for the size range considered (i.e., N = 24−28) was that among all the data on $(pH_2)_N$ clusters reported previously, ref 12 using DMC-IS with the most accurate IS wavefunction seems to be the most reliable both quantitatively and qualitatively. However, in order to obtain accurate results for larger sizes N > 28, the DMC-IS calculations should be revisited using much larger population sizes N_w with the hope of circumventing the curse of dimensionality.

AUTHOR INFORMATION

Corresponding Author

Vladimir A. Mandelshtam − *Department of Chemistry, University of California, Irvine, Irvine, California 92697, United States;* orcid.org/0000-0001-6395-1397; Email: mandelsh@uci.edu

Author

Bridgett H. Kohno − *Department of Chemistry, University of California, Irvine, Irvine, California 92697, United States;* orcid.org/0000-0001-5366-1476

Complete contact information is available at: https://pubs.acs.org/10.1021/acs.jpca.0c07107

Notes

The authors declare no competing financial interest.

ACKNOWLEDGMENTS

This work was supported by the National Science Foundation (NSF) (grant CHE-1900295). We are grateful to Joel Mallory for sharing with us some of his codes and expertise.

https://dx.doi.org/10.1021/acs.jpca.0c07107
J. Phys. Chem. A 2020, 124, 8766−8777

REFERENCES

(1) Maris, H. J.; Seidel, G. M.; Huber, T. E. Supercooling of liquid H_2 and the possible production of superfluid H2. *J. Low Temp. Phys.* **1983**, *51*, 471−487.
(2) Sindzingre, P.; Ceperley, D. M.; Klein, M. L. Superfluidity in clusters of p-H_2 molecules. *Phys. Rev. Lett.* **1991**, *67*, 1871−1874.
(3) Silvera, I. F.; Goldman, V. V. The isotropic intermolecular potential for H_2 and D_2 in the solid and gas phases. *J. Chem. Phys.* **1978**, *69*, 4209.
(4) Buck, U.; Huisken, F.; Kohlhase, A.; Otten, D.; Schaefer, J. State resolved rotational excitation in D_2+H_2 collisions. *J. Chem. Phys.* **1983**, *78*, 4439−4450.
(5) Doye, J. P. K.; Calvo, F. Entropic effects on the structure of lennard-jones clusters. *J. Chem. Phys.* **2002**, *116*, 8307−8317.
(6) Predescu, C.; Frantsuzov, P. A.; Mandelshtam, V. A. Thermodynamics and equilibrium structure of Ne_{38} cluster: Quantum mechanics versus classical. *J. Chem. Phys.* **2005**, *122*, 154305.
(7) Deckman, J.; Mandelshtam, V. A. Effects of quantum delocalization on structural changes in Lennard-Jones clusters. *J. Phys. Chem. A* **2009**, *113*, 7394.
(8) Sevryuk, M. B.; Toennies, J. P.; Ceperley, D. M. Why are para-hydrogen clusters superfluid? a quantum theorem of corresponding states study. *J. Chem. Phys.* **2010**, *133*, No. 064505.
(9) Warnecke, S.; Sevryuk, M. B.; Ceperley, D. M.; Toennies, J. P.; Guardiola, R.; Navarro, J. The structure of para-hydrogen clusters. *Eur. Phys. J. D* **2010**, *56*, 353−358.
(10) Mallory, J. D.; Mandelshtam, V. A. Quantuminduced solid-solid transitions and melting in the lennard-jones LJ_{38} cluster. *J. Chem. Phys.* **2018**, *149*, 104305.
(11) Guardiola, R.; Navarro, J. Structure of small clusters of parahydrogen molecules. *Phys. Rev. A* **2006**, *74*, No. 025201.
(12) Guardiola, R.; Navarro, J. A diffusion monte carlo study of small para-hydrogen clusters. *Open Phys.* **2008**, *6*, 33−37.
(13) Sola, E.; Boronat, J. Solidification of small p-H2 clusters at zero temperature. *J. Phys. Chem. A* **2011**, *115*, 7071−7076.
(14) Mallory, J. D.; Mandelshtam, V. A. Quantum melting and isotope effects from diffusion Monte Carlo studies of *p*-H_2 clusters. *J. Phys. Chem. A* **2017**, *121*, 6341.
(15) Khairallah, S. A.; Sevryuk, M. B.; Ceperley, D. M.; Toennies, J. P. Interplay between magic number stabilities and superfluidity of small parahydrogen clusters. *Phys. Rev. Lett.* **2007**, *98*, 183401.
(16) Cuervo, J. E.; Roy, P.-N. Path integral ground state study of finite-size systems: Application to small $(parahydrogen)_n$ (n=2-20) clusters. *J. Chem. Phys.* **2006**, *125*, 124314.
(17) Cuervo, J. E.; Roy, P.-N. On the solid- and liquidlike nature of quantum clusters in their ground state. *J. Chem. Phys.* **2008**, *128*, 224509.
(18) Cuervo, J. E.; Roy, P.-N. Weakly bound complexes trapped in quantum matrices: Structure, energetics, and isomer coexistence in $(para\text{-}H_2)_n(ortho\text{-}D_2)_3$ clusters. *J. Chem. Phys.* **2009**, *131*, 114302.
(19) Mezzacapo, F.; Boninsegni, M. Superfluidity and quantum melting of p-H_2 clusters. *Phys. Rev. Lett.* **2006**, *97*, No. 045301.
(20) Mezzacapo, F.; Boninsegni, M. Structure, superfluidity, and quantum melting of hydrogen clusters. *Phys. Rev. A* **2007**, *75*, No. 033201.
(21) Boninsegni, M.; Moroni, S. Population size bias in diffusion Monte Carlo. *Phys. Rev. E* **2012**, *86*, No. 056712.
(22) Schmidt, M.; Constable, S.; Ing, C.; Roy, P.-N. Inclusion of trial functions in the langevin equation path integral ground state method: Application to parahydrogen clusters and their isotopologues. *J. Chem. Phys.* **2014**, *140*, 234101.
(23) Miura, S. Quantum structural fluctuation in parahydrogen clusters revealed by the variational path integral method. *J. Chem. Phys.* **2018**, *148*, 102333.
(24) Hoare, M. R.; Pal, P. Physical cluster mechanics: Statics and energy surfaces for monatomic systems. *Adv. Phys.* **1971**, *20*, 161−196.
(25) Northby, J. Structure and binding of lennard-jones clusters: 13 ≤n≤ 147. *J. Chem. Phys.* **1987**, *87*, 6166.
(26) Doye, J. P. K.; Miller, M. A.; Wales, D. J. The doublefunnel energy landscape of the 38-atom Lennard-Jones cluster. *J. Chem. Phys.* **1999**, *110*, 6896.
(27) Sharapov, V. A.; Meluzzi, D.; Mandelshtam, V. A. Low-temperature structural transitions: Circumventing the broken-ergodicity problem. *Phys. Rev. Lett.* **2007**, *98*, 105701.
(28) Rabani, E.; Jortner, J. Spatial delocalization in *para* H_2 clusters. *J. Phys. Chem. B* **2006**, *110*, 18893.
(29) Mezzacapo, F.; Boninsegni, M. Classical and quantum physics of hydrogen clusters. *J. Phys.: Condens. Matter* **2009**, *21*, 164205.
(30) Mezzacapo, F.; Boninsegni, M. Parahydrogen clusters: Numerical estimates and physical effects. *J. Phys.: Conf. Ser.* **2009**, *150*, 032059.
(31) Steinhardt, P. J.; Nelson, D. R.; Ronchetti, M. Bondorientational order in liquids and glasses. *Phys. Rev. B* **1983**, *28*, 784−805.
(32) Anderson, J. B. A random-walk simulation of the schrödinger equation: H_3^+. *J. Chem. Phys.* **1975**, *63*, 1499.
(33) Anderson, J. B. Quantum chemistry by random walk. H^2P, H_3^+ D_{3h} $1A_1^{'}$, H_2 $^3\sigma_u^+$, H_4 $^1\sigma_g^+$, Be ^1S. *J. Chem. Phys.* **1976**, *65*, 4121.
(34) M. E. J., Newman; G. T., Barkema, *Monte Carlo Methods in Statistical Physics* Oxford University Press, 1990.
(35) Mandelshtam, V. A.; Frantsuzov, P. A. Multiple structural transformations in Lennard-Jones clusters: Generic versus size-specific behavior. *J. Chem. Phys.* **2006**, *124*, 204511.
(36) Doye, J. P. K.; Wales, D. J. The structure and stability of atomic liquids: From clusters to bulk. *Science* **1996**, *271*, 484−487.

https://dx.doi.org/10.1021/acs.jpca.0c07107
J. Phys. Chem. A 2020, 124, 8766−8777